Scanning Long-wave Optical Test System – a new ground optical surface slope test system

Tianquan Su*, Won Hyun Park, Robert E. Parks, Peng Su, James H. Burge
College of Optical Sciences, The University of Arizona, Tucson, Arizona 85721, USA

ABSTRACT

The scanning long-wave optical test system (SLOTS) is under development at the University of Arizona to provide rapid and accurate measurements of aspherical optical surfaces during the grinding stage. It is based on the success of the software configurable optical test system (SCOTS) which uses visible light to measure surface slopes. Working at long wave infrared (LWIR, 7-14 um), SLOTS measures ground optical surface slopes by viewing the specular reflection of a scanning hot wire. A thermal imaging camera collects data while motorized stages scan the wire through the field. Current experiments show that the system can achieve a high precision at micro-radian level with fairly low cost equipment. The measured surface map is comparable with interferometer for slow optics. This IR system could be applied early in the grinding stage of fabrication of large telescope mirrors to minimize the surface shape error imparted during processing. This advantage combined with the simplicity of the optical system (no null optics, no high power carbon dioxide laser) would improve the efficiency and shorten the processing time.

Key Words: optical testing, reflection deflectometry, long wave infrared, ground surface, slope measurement

1. INTRODUCTION

The scanning long-wave optical test system (SLOTS) is developed on the demand of measuring large optics during the grinding stage, so that the surface shape error during fabrication can be corrected earlier and faster. The ground optical surface before polishing is diffuse to visible light, but appears more specular with longer wavelength light. SLOTS applies the same principle as SCOTS, but uses LWIR (7-14 um) equipment. A thermal imaging camera is used. A scanning hot wire serves as the light source. It is used to measure glass surfaces ground with 20 um and finer loose abrasive grit.

SLOTS is developed based on the success of the software configurable optical test system (SCOTS). SCOTS is a rapid, robust and accurate system for measuring highly aspherical surfaces using specular reflection in visible wavelength. It applies the principle of the Hartmann test in reverse. In SCOTS, a camera with small aperture images the surface under test; an LCD screen provides programmable illumination. The slope data can be integrated using polynomial fitting or zonal integration methods. High-performance results are achieved with loose tolerance by measuring optical surfaces from their center of curvature. The results from SCOTS have been proven comparable with interferometric tests [1].

In this paper, the general principle of reflection slope test and the mechanism of the LWIR system are described in the second section. The factors affecting the precision and accuracy are listed in the third section. Measurements of several surfaces with different radii of curvatures are demonstrated.

2. PRINCIPLES

2.1 Slope measurement using specular reflection

SLOTS tests surfaces using specular reflection. Imaging one ray from a point source hits a point on the mirror (a "mirror point"), and is reflected into a pinhole camera. The norm of the mirror point will be the bisector of the angle made by the

* tsu@optics.arizona.edu

Optical Manufacturing and Testing IX, edited by James H. Burge, Oliver W. Fähnle, Ray Williamson,
Proc. of SPIE Vol. 8126, 81260E · © 2011 SPIE · CCC code: 0277-786X/11/$18 · doi: 10.1117/12.892666

incident and the reflected rays. See Figure 1. The local slope of that "mirror point" can be calculated with the coordinates of the source, the aperture and the "mirror point". The position of the "mirror point" is unknown as it is the purpose of the measurement. But because the ideal shape of optical surfaces are usually known and the departure from ideal shape is very small, the ideal position of the "mirror point" is used in the calculation. For convenience of calculation and process, the surface slope is decomposed into two orthogonal directions defined as x and y. See Eq (1) [2].

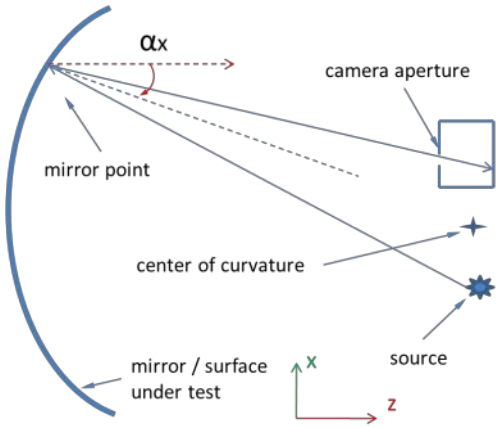

Figure 1 The schematic plot shows the idea of measure the surface slope using specular reflection.

$$\tan\alpha_x(x_m, y_m) = \frac{\frac{x_m - x_s}{d_{m2s}} + \frac{x_m - x_c}{d_{m2c}}}{\frac{z_{m2s} - W(x_m, y_m)}{d_{m2s}} + \frac{z_{m2c} - W(x_m, y_m)}{d_{m2c}}} \quad (1)$$

$$\tan\alpha_y(x_m, y_m) = \frac{\frac{y_m - y_s}{d_{m2s}} + \frac{y_m - y_c}{d_{m2c}}}{\frac{z_{m2s} - W(x_m, y_m)}{d_{m2s}} + \frac{z_{m2c} - W(x_m, y_m)}{d_{m2c}}}$$

Where x_m and y_m are the coordinates of the "mirror point"; x_c and y_c are the coordinates of the camera aperture; x_s and y_s are the coordinates of the source; z_{m2s} and z_{m2c} are the z direction distances from the mirror vertex to the source and the mirror between the camera aperture; d_{m2s} and d_{m2c} are the distances from the mirror pixel to the source and the camera aperture; $W(x_m, y_m)$ is the surface sag function.

There are two conjugate relations in the system. The first one is the 1:1 conjugation between the camera aperture and the source, established by placing the camera and the source close to the center of curvature (CoC) of the mirror under test. By placing the system near the CoC of the mirror, where the derivative of the ray slope is close to zero, the sensitivity to camera lens distortion is greatly reduced. The second conjugation is between the camera detector and the mirror under test, established by focusing the camera on the mirror. By doing so, the camera maps the mirror to the detector. Each detector pixel corresponds to a small area on the mirror, which will be called a "mirror pixel" in the following discussion. The source can only illuminate certain detector pixel when it is on the reflection line of the line connecting the detector and the corresponding "mirror pixel". When the detector is illuminated, the average slope of that "mirror pixel" can be calculated with the coordinates of the "mirror pixel", the pinhole and the source.

Using one point source in measurements will be time consuming, as measuring the whole mirror surface requires moving the source around to illuminate each detector pixel. For a substitution, a line source can be scanned in two orthogonal directions (x and y) to measure the surface slope in two directions during which the position of the source can be described with a single value in x or y at any instant moment.

For finite size camera aperture and source, centroiding in source coordinate is used to obtain the source position x_s and y_s. In real measurements, the camera aperture is of finite size to avoid shutting out all the light and lowering the

diffraction effect. The camera aperture is imaged by "mirror pixels" onto the source plane. If the line source is located at the aperture image, the source will illuminate the corresponding detector pixels. See Figure 2.

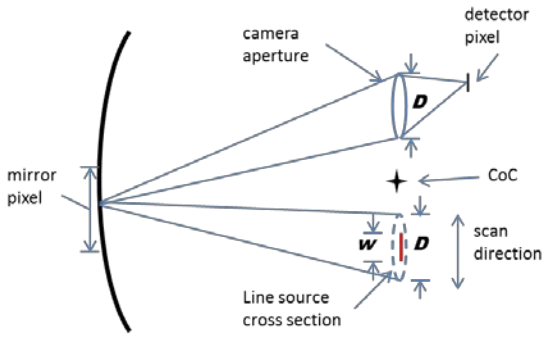

Figure 2. The camera aperture is imaged onto the source plane by a certain "mirror pixel". When the source is located at the aperture image, it can illuminate the corresponding detectro pixel. The camera aperture diameter is D; the line source width is w.

Meanwhile, the line source is also imaged onto the camera aperture. As the image of the line source moves across the camera aperture, the amount of the source image going into the camera increases first, and then drops back to zero. See Figure 3 (a). If the radiative energy falling on this detector pixel is plotted versus the movement of the line source, a curve like Figure 3 (b) can be obtained.

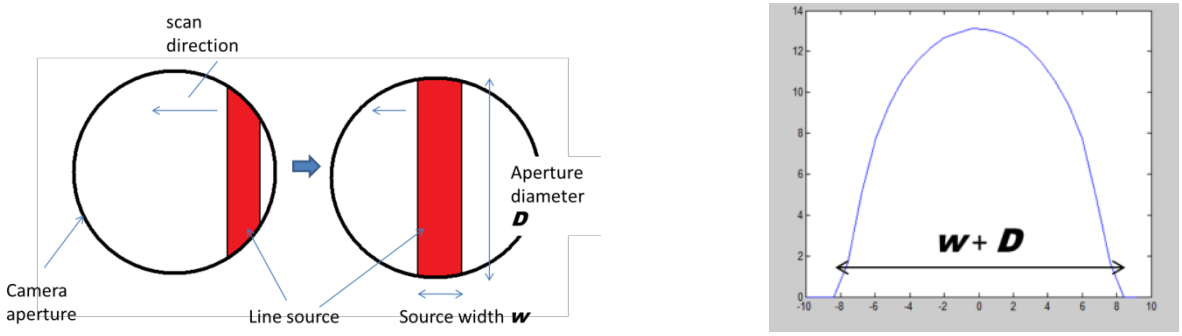

(a) (b)

Figure 3 (a) The source image seen by a single detector pixel as it scans across the camera aperture. (b) A simulated plot of the intensity change of the single detector pixel. The x-axis is the position of the source; the y-axis is the intensity readout of the detector pixel. In the simulation, the aperture is circular and the wire width is smaller than the aperture diameter.

The curve in Figure 3 (b) above is sampled during the measurement by taking pictures with the camera. Then, centroiding is used to determine the source position in Eq (1). See Eq (2).

$$x_s = \frac{\sum x_i I_i}{\sum I_i} \; ; \qquad y_s = \frac{\sum y_i I_i}{\sum I_i} \tag{2}$$

Where x_i and y_i are the coordinates of the source at scan step i; I_i is the corresponding detector readout. Note that the centroiding is done in source coordinates, not on the detector plane.

The radiative energy falls on the detector is determined by the radiance of the source, the specular reflectivity of the mirror, the diameter of the camera aperture and the width of the line source. Figure 4 shows the radiometry relation of the system.

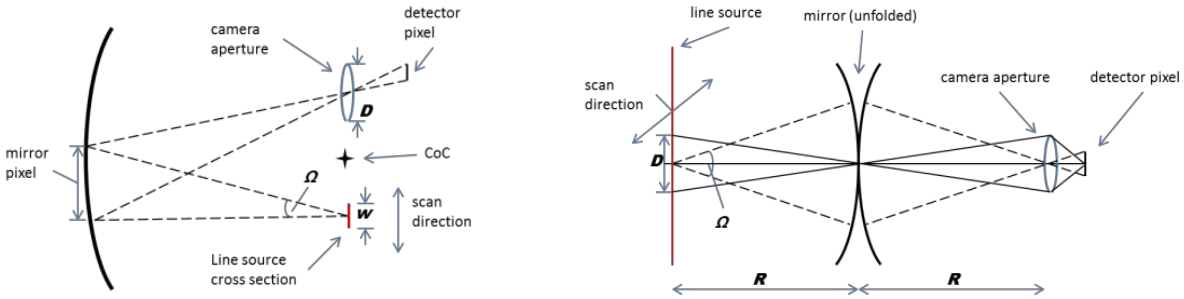

(a) (b)

Figure 4. The plots show the radiometry relations between the source and the detector. Plot (a) is the setup seen along the length of the line source. Plot (b) unfolds the system about the mirror under test, and is seeing along the scan direction of the source.

The maximum size of the source that can be seen by one single pixel is determined by the camera aperture D and the width of the line source w, assuming $D > w$. The line source overfills the camera aperture in one direction and underfills in another. Both Figure 3 and Figure 4 show the idea. When the source image is at the center of the aperture, the maximum source area, $A = wD$, is reached.

The cone of light Ω collected from one point source is determined by the mirror pixel size and the radius of the mirror R, which is further determined by the instantaneous FOV of one detector pixel (IFOV). As the source plane is 1:1 conjugate to the camera aperture plane, the solid angle Ω extended by the "mirror pixel" from the point source is the same as the IFOV of the detector pixel. Note that, the solid angle will not change with the radii of different mirrors under test, as long as the system is always placed at the center of curvature.

With all the information above, the radiative flux on one single pixel can be calculated with the radiometry equation:

$$\Phi = \mathrm{r}LA\Omega = rL\Omega wD \qquad (3)$$

Where r is the specular reflectivity of the mirror; L is the radiance of the source; w is the width of the source; D is the diameter of the camera aperture; Ω is the solid angle of the light collected from one point source, which is equal to the IFOV of the detector pixel.

2.2 Work in Long Wave Infrared (LWIR)

To obtain enough specular reflection from the surface, the working wavelength needs to be much longer than the surface roughness [3]. The working wavelength of most LWIR detector available is within 7-14 um. Light in this band is able to measure a surface roughness about 1um rms which is too scattering in visible band (0.3-0.7 um). Common optical glasses are opaque in LWIR band. The reflectivity of glass surface at 10 um is about 25% for normal incidence [4], which is higher than the 4% in visible band. The specular reflection decreases as the surface roughness increases. Figure 5 shows the measured specular signal from surfaces ground by different grits.

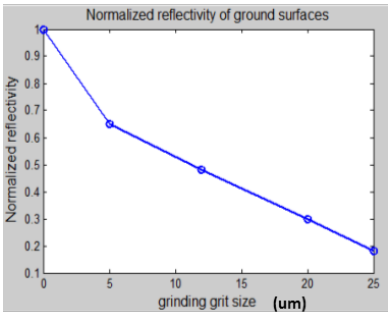

Figure 5. Measured specular reflectivity in 7-14 um band for ground surfaces. The values are normalized to the polished surface. The five data circles in the plot were obtained by measure surfaces with different finish: polished, 5um, 12um, 20um and 25um grit ground.

A LWIR camera with uncooled microbolometer focal plane array (FPA) is used in SLOTS. Each pixel of the microbolometer is a temperature-sensitive electrical resistor. The sensitive material on the pixel absorbs the incident radiation, which lead to a self-temperature raise. The pixel electrical resistance then changes with the temperature. A readout circuit reads the pixel voltage change, and converts it to digitized signals. The sensitive material temperature fluctuation is the fundamental source of the noise [5]. Figure 6 shows an example of thermal imaging.

Figure 6. A picture taken by thermal imaging camera. In this picture, bright means hot. The human face appears brighter as its temperature is higher than the surroundings.

According to Planck's law of blackbody radiation, high temperature object can be used as the light source in LWIR. The radiative spectral energy distribution will be a function of the object temperature. See Figure 7 (a). At room temperature (300K), the radiation peak is within the LWIR band (7-14 um). As the temperature increases, the radiation peak will shift towards the shorter wave length. But the integrated energy in LWIR will always increase with the source temperature. See Figure 7 (b).

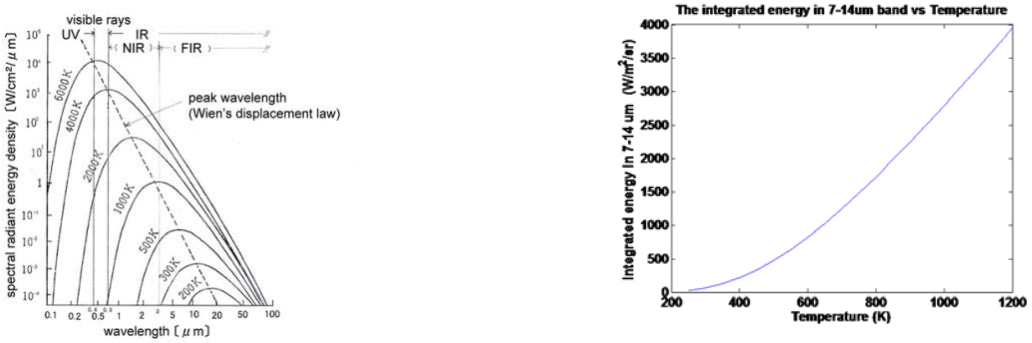

(a) (b)

Figure 7. (a) Blackbody radiation curves. Each curve shows the spectral radiative energy distribution at a certain temperature. (b) The integrated energy in 7-14 um band at different temperatures. The curve is almost linear beyond 600 K.

The high temperature source can be obtained from Joule heat by electrically heating a metal wire. The total energy consumed is given by Joule's law, see Eq (4):

$$P = I\,V = I^2R = V^2/R \tag{4}$$

The radiative energy emitted will depend on the temperature of the wire and its spectral emissivity.

3. PRECISION AND ACCURACY ANALYSIS

It can be seen from Eq (1) that the system precision (repeatability) and the accuracy of the system both rely on the geometric measurements of those parameters. The precision is affected by the noise from the camera, the precision of the scan system, and other random effects. The accuracy is affected by the camera lens distortion, the pupil aberration, and some other factors that are still or change very lowly.

3.1 Precision Analysis: uncertainty of centroiding

The slope is calculated by the source centroid (x_s and y_s) over the distance from the mirror to the source (R), so the centroiding directly affect the precision, as x_s and y_s are the only parameters in Eq (1) that change from measurement to measurement. The analysis of centroiding is discussed a lot for Hartmann-Shack wavefront sensor [6-9]. See Eq (5). It only considered the error in I_i in Eq (2). The error of the scan system that goes to x_i in Eq (2) is not included.

$$\sigma_{x_s}^2 = \frac{(w+D)^2}{\sum_i^N I_i}\left(1+\frac{\sigma_r^2}{\bar{I}}\right) = \frac{(\mathrm{w}+\mathrm{D})^2}{N\bar{I}}\left(1+\frac{\sigma_r^2}{\bar{I}}\right) \quad (5)$$

Where $w + D$ is the width of the intensity curve shown in Figure 3. N is the number of the samples on the intensity curve. It is the number of pictures taken while the source image scans through the camera aperture. σ_r is the combined noise, which can be obtained by measurement. $\bar{I}$ is the averaged intensity in each sample.

The error introduced by the stages movement is very small. The error goes into the x_i and y_i in Eq (2), so that affects the centroiding. The error in x_i comes from the precision of the linear stage, the vibration of the heat wire, the instability of the camera frame rate. Because the accuracy of the stepper motor stages is at um level, and the stability of the camera video frame rate is at 0.1 fps, the error is below one um. With a mirror with 1 m radius of curvature, the error will below a few tenths of microradian, which is negligible in the current system.

3.2 Accuracy: List of Sources

Camera lens distortion will degrade the mapping between the detector and the mirror. The image may not be able to reflect the true shape of the mirror. When testing fast optics, large FOV lenses are needed, so the distortion is likely to be considerable. But it can be calibrated by photogrammetric methods.

The pupil aberration affect the measurement by introduce error into x_c and y_c in Eq (1). During the data reduction, the center of the first camera lens is used as the coordinate of the camera, assuming that the entrance pupil locates at the first element and all the 1st order specular reflection (chief rays) go through the same point. This will not be true if the entrance pupil is not locate at the first element of the lens or even not well defined. The deviation of reality from the calculation will bring field dependent errors into the measurement. This will affect the low order terms if the surface measurements is fit with polynomials. One way to solve the problem is to use customized lenses. A design with well-defined entrance pupil and small aperture is preferred. It would be ideal if the stop of the lens is placed in the front of the camera.

The wire bending affects the measurement by bringing repeatable error into x_s and y_s in Eq(1). If the wire is bent or sags, the centroid will be shifted. It can be controlled to a negligible level by keeping proper tension on the wire during measurements.

4. EXPERIMENTS

The SLOTS equipment is shown in Figure 8. The camera used is an uncooled microbolotmeter thermal imaging camera. The source is an electrically heated tungsten wire. The wire can be moved by the scanning system consists of linear stages. A rotary stage (not shown) rotates the wire to keep it perpendicular to the scanning direction. A computer controls the camera and the scanning system.

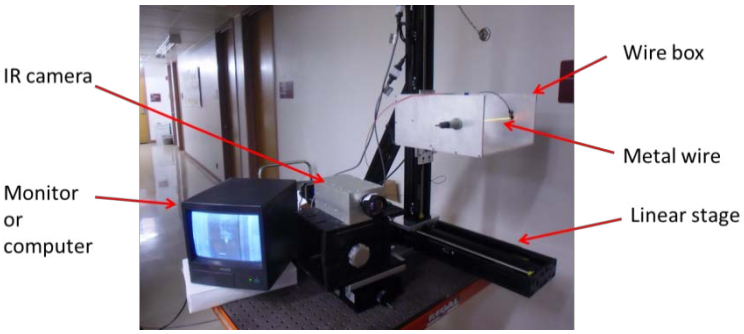

Figure 8. The equipment of SLOTS.

The wire source is mounted on a metal box to provide a cool and uniform background. In LWIR band, smooth finished metals, like the stage carrier, are highly reflective that can generate ghost images of the source. The ghost images will degrade centroiding accuracy. The wire box is designed to guide, with a tilted metal surface, the backwards emitting light to an open space where free of metal structures or thermal sources. See Figure 9.

(a) (b)

Figure 9. (a) The wire box guides the backwards emitting light away from the surface under test. (b) The actual wire box.

As discussed in section 2, the detector is illuminated when the source is placed at the image of the camera aperture. Figure 10 shows a picture from the IR camera, compared with the visible picture. The mirror appears bright as it reflects the radiation from the source, instead of has a high temperature itself.

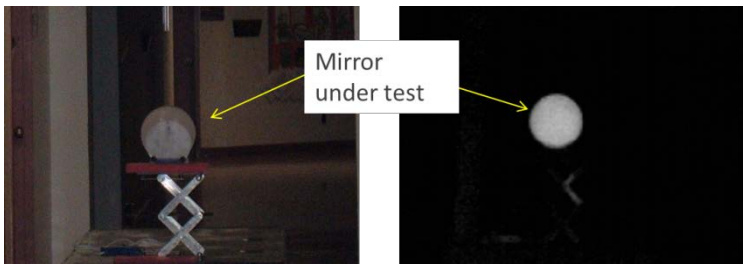

Figure 10. The measurement of a ground surface mirror. The left picture is taken by normal camera; the right one is taken by thermal imaging camera. The mirror appears bright in the thermal image not because its temperature is higher than the surroundings, but that it reflects light of the heat source into the camera.

A cross-shaped camera aperture is used to improve the measurement precision. As discussed in section 3.1, the uncertainty is proportional to the sum of the camera aperture size D and the wire width w. Moreover, the radiometry model in section 2 shows that in the scanning direction the width of the wire determines the energy instead of the aperture diameter. Therefore, a cross-shaped camera aperture is designed to narrow the centroiding range, block part of the background noise, and still pass all the signal. Figure 11 shows the idea and the design. The effect on centroiding can be seen in Figure 12.

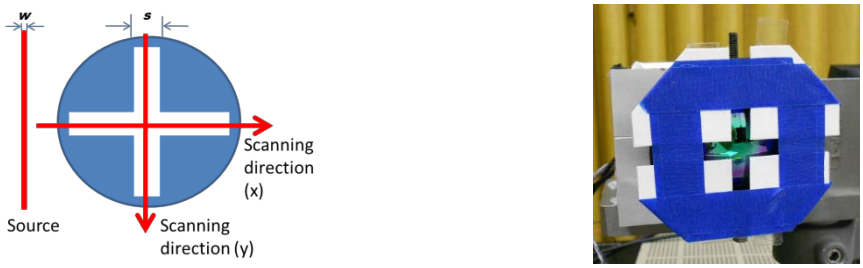

(a) (b)

Figure 11. (a) The schematic plot shows the idea of the cross shaped camera aperture. (b) The prototype made with cardboard is used in measurements.

With the equipment above, several measurements were done for different surfaces. The measured surfaces included a polished mirror and three 20um ground mirrors, all with different radii of curvature. The main performance figure of merit at this moment is precision (repeatability). Table 1 shows the parameters in the experiment. Table 2 shows the specs of the measured surfaces.

Table 1. The experiment parameters

wire material	Tungsten	**camera frame rate**	15 fps
wire current/volts	7A/6V	**camera FOV**	9X12 deg
wire dimension	2.5 X 300 X 0.2 mm	**scanning speed**	10 mm/s
camera resolution	320 X 240	**scanning pitch**	0.667 mm
camera aperture size	15X40 mm		

Table 2. Measured surfaces specs

Radius of Curvature	surface finish	surface diameter
1.9m	polished	4 inch
1.6m	20 um loose abrasive ground	4 inch
9m	20 um loose abrasive ground	6 inch
19m	20 um loose abrasive ground	4 inch

The signal profile of one single detector pixel is shown in Figure 12. The profile is about 17mm wide, equaling the total width of the camera aperture and the wire. As the wire is thinner than the aperture, $s > w$, the wire image under-fill the aperture, which makes "flat top" in the profile. A threshold and a "window" are used to eliminate background noise that is outside the expected centroiding range. Then the measured data were interpolated to obtain a better centroiding result. Shown in Figure 12, only the crosses were used for centroiding.

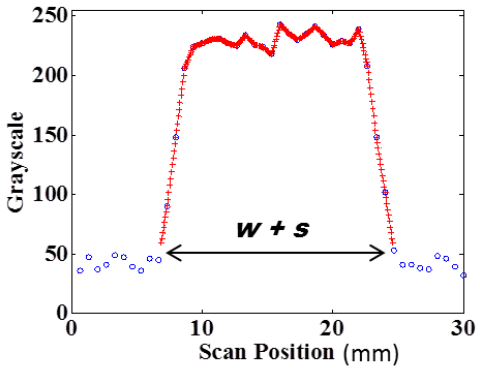

Figure 12. The measured intensity curve of one detector pixel. The x-axis is the position in mm, while the y-axis is the 8-bit detector grayscale. The blue circles represent real measurements; the red crosses represent interpolated data. The width of the curve equals the sum of the width of the wire (w) and the width of the camera aperture slot (s). The "flat top" comes from the smaller wire width than the camera aperture.

The measurement results are shown in Table 3. The results show that SLOTS reaches a precision of microradian level. The polished mirror is measured in two directions and the surface map is compared with an interferometer test.

Table 3. Measurement results

Radius of curvature / finish	Imaging resolution	W+S	SNR	Centroid precision (10 averaged)	Slope precision (10 averaged)
1.9m polish	1 mm	17.5 mm	63	2.85 um	1.5 urad
1.6m ground	0.8 mm	17.5 mm	45	4.64 um	2.9 urad
9m ground	4.5 mm	17.5 mm	34	7.2 um	0.8 urad
19m ground	10 mm	17.5mm	29	9.5 um	0.5 urad

The slope is calculated from the centroid and the distance R. The slope repeatability is proportional to the centroid repeatability, because the angle variation is small. One can see that the centroid variation increase with the distance. This is related to the SNR decreasing with the distance. The results generally match Eq (5).

The polished surface result is compared with the interferometry result, and these two reach a high agreement. The obtained slope map is fitted with derivative of the Zernike polynomials [10]. The surface map can be obtained by zonal integration. Figure 13 shows the measurement results of the polished mirror from SLOTS and interferometer respectively. The first ten Zernike terms are removed as they can be affected greatly by the alignment. A pixel-to-pixel subtraction is also shown.

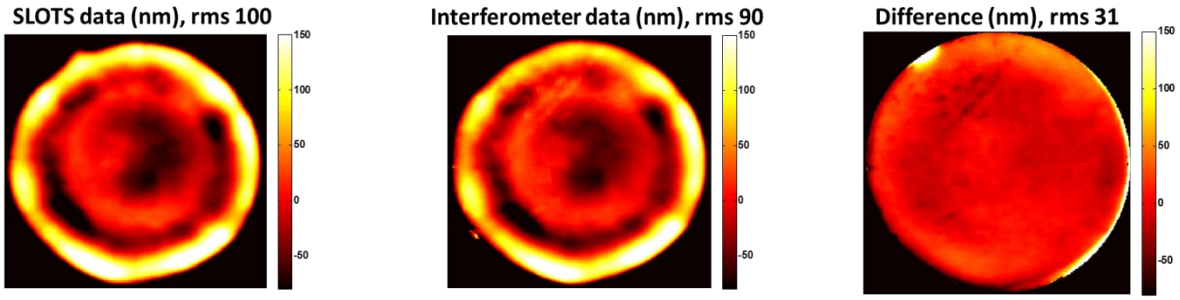

Figure 13. Compare of the surface maps from SLOTS and interferometer. The subtraction is not perfectly aligned, so the actual difference between the two maps is smaller than 31nm rms.

5. SUMMARY

SLOTS is a ground surface slope test system developed on the base of SCOTS. It works in the LWIR band to make specular measurements on ground optical surfaces. This paper describes the working mechanism and the radiometry model of the system. The principles and the equipment related to LWIR are also introduced. It shows how the line-scanning and the centroiding techniques are applied, and how they affect the measurement precision. The factors that affect the accuracy are also listed.

The experiments show that with current system the precision reaches micro-radian level on mirrors with 20um grit ground surface. With a spatial resolution of a few millimeters, SLOTS is able to measure a surface height variation in tens of nanometer level. With careful calibration, SLOTS should be able to provide a robust measurement during the grinding stage of the large optics process. The visual compare between the SLOTS data and the interferometer indicates the promise. Besides optical surface test, it is also possible to apply SLOTS on some other rough surface measurements, such as car-body shape detection before painting.

The authors are grateful for support from NIST, U.S. Dept. of Commerce, under ARRA Award #60NANB10D010.

REFERENCES

[1] Su, P., Parks, R. E., Wang, L., Angel, R. P. and Burge, J. H., "Software configurable optical test system – computerized reverse Hartmann test". Applied Optics. Vol. 49, No. 25(2010)

[2] Ritter, R., Hahn, R., "Contribution to analysis of the reflection grating method". Optics and Lasers in Engineering 4 13-24. (1983)

[3] Stover, J., "Roughness characterization of smooth machined surfaces by light scattering," Appl. Opt. 14, 1796-1802 (1975)

[4] Hsieh, C. K. , Su. K. C. , "Thermal radiative properties of glass from 0.32 to 206 um". Solar Energy. Vol.22, pp. 37-43. (1978)

[5] Kruse. P. W., [Uncooled Thermal Imaging: arrays, systems ,and applications]. SPIE PRESS. Tutorial Texts in Optical Engineering V. TT51 (2001)

[6] Neal, D. R., Copland, J., and Neal, D., "Shack-Hartmann wave front sensor precision and accuracy". Proc. SPIE 4779, (2002)

[7] Morgan, J. S., Slater, D. C., Timothy, J. G., and Jenkins, E. B., "Centroid position measurements and sub-pixel sensitivity variations with MAMA detector", Appl. Opt. Vol. 28, No.6 (1989)

[8] Cao, G., Yu, X., "Accuracy analysis of a Hartmann-Shack wavefront sensor operated with a faint object". Opt. Eng. Vol. 33 No.7. (1994)

[9] Thomas, S., Fusco, T., Tokovinin, A., Nicolle, M., Michau. V. , and Rousset. G., "Comparison of centroid computation algorithms in a Shack-Hartmann sensor", Mon. Not. R. Astron. Soc. 371, 323-336 (2006)

[10] Malacara-Doblado, D., and Ghozeil, I. "Hartmann, Hartmann-Shack, and Other Screen Tests", in [Optical Shop Testing] 3rd ed., Wiley Series in Pure and Applied Optics (Wiley, 2007), pp. 361-397.